Published in final edited form as:
Int J Hyperthermia. 2012 ; 28(5): 456–465. doi:10.3109/02656736.2012.677931.

Miniature Microwave Applicator for Murine Bladder Hyperthermia Studies

Sara Salahi, **Paolo F. Maccarini**, **Dario B. Rodrigues**, **Wiguins Etienne**, **Chelsea D. Landon**, **Brant A. Inman**, **Mark W. Dewhirst**, and **Paul R. Stauffer**

Abstract

Purpose—Novel combinations of heat with chemotherapeutic agents are often studied in murine tumor models. Currently, no device exists to selectively heat small tumors at depth in mice. In this project, we modelled, built and tested a miniature microwave heat applicator, the physical dimensions of which can be scaled to adjust the volume and depth of heating to focus on the tumor volume. Of particular interest is a device that can selectively heat murine bladder.

Materials and Methods—Using Avizo® segmentation software, we created a numerical mouse model based on micro-MRI scan data. The model was imported into HFSS™ simulation software and parametric studies were performed to optimize the dimensions of a water-loaded circular waveguide for selective power deposition inside a 0.15ml bladder. A working prototype was constructed operating at 2.45GHz. Heating performance was characterized by mapping fiber-optic temperature sensors along catheters inserted at depths of 0-1mm (subcutaneous), 2-3mm (vaginal), and 4-5mm (rectal) below the abdominal wall, with the mid-depth catheter adjacent to the bladder. Core temperature was monitored orally.

Results—Thermal measurements confirm the simulations which demonstrate that this applicator can provide local heating at depth in small animals. Measured temperatures in murine pelvis show well-localized bladder heating to 42-43°C while maintaining normothermic skin and core temperatures.

Conclusions—Simulation techniques facilitate the design optimization of microwave antennas for use in pre-clinical applications such as localized tumor heating in small animals. Laboratory measurements demonstrate the effectiveness of a new miniature water-coupled microwave applicator for localized heating of murine bladder.

Keywords

hyperthermia; bladder hyperthermia; microwave applicator; small animal heating systems

Introduction

Superficial bladder cancer is currently treated with intravesicular chemotherapy, using mitomycin-C (MMC). However, as with other chemotherapy drugs, tumor cells eventually develop a resistance to MMC, rendering the treatment less effective or completely ineffective (1). *In vitro* studies have shown that the application of hyperthermia (increasing temperature to 41-43°C) to cancer cells increases their sensitivity to MMC and reverses MMC resistance (2). A recent 18-patient pilot study demonstrated a safe and reliable method

Corresponding Author: Sara Salahi, 136 Hudson Hall, Box 90281, Durham, NC 27708, (919) 668-1980 sara.salahi@duke.edu.

Declaration of Interest
The authors report no conflict of interest.

for heating bladder to 40-43°C as an adjuvant therapy during MMC treatments (3). Given the promising implications of this study, we are now interested in using established murine bladder cancer models to study the mechanisms behind the increased effectiveness observed in combination hyperthermia and intravesicular MMC treatments in order to better assess the future potential of such combinatory treatment protocols.

The most commonly used method for inducing hyperthermia in murine tumor models is to submerse the tumor bearing portion of the mouse into a hot water bath (4-8). Since this method cannot provide selective power deposition into tissues at depth, it has been useful mainly for tumors in the hind limb where the region immersed can be limited primarily to the target tumor mass. Water bath heating of murine bladder would require circulation of heated water through the bladder or submersing the lower half of the mouse's body. The former is not technically achievable for a 0.15ml bladder and the latter would heat the entire hind quarter of the mouse. This would elevate the mouse's central body temperature to dangerous levels, which could be toxic. Other methods for locally heating deep seated organs like the urinary bladder have been explored. A few examples include ultrasound transducers (9) and RF heating with parallel-plate configurations (10) which have been shown to effectively heat superficial murine flank tumors. Ferrite powder (11, 12), water-based ferrofluids (13), or iron oxide nanoparticles (14) could be instilled into the bladder, which would then heat up with the application of an external magnetic field. Although potentially effective, these methods are expensive and may require invasive methods to effectively deliver the metal powders and particles to the region of interest.

This work presents a simulation-based approach to antenna design for pre-clinical hyperthermia studies. Before electromagnetic simulation techniques were available, microwave antenna optimization was accomplished through an iterative build-and-test method and some scientists still employ this method, while others use advanced simulation techniques to reduce the overall cost and time required to develop a new device from concept to working product. HFSS™ (Ansys Inc., Canonsburg, PA) is an effective simulation tool for designing antennas. It employs the finite-element method to approximate the solution to the partial differential equations that define electromagnetic wave propagation and power deposition in different media. HFSS™ and other electromagnetic simulation software packages are often used to predict power deposition in patients for hyperthermia treatment planning (15-17) where accurate 3-dimensional (3D) anatomical models of patients are employed. This study uses the same methods to design an antenna with optimal performance based on the results of parametric electromagnetic studies in HFSS™ as well as thermal studies in COMSOL Multiphysics® (COMSOL Inc., Burlington, MA) in a 3D numerical murine model.

This approach to antenna optimization for pre-clinical hyperthermia devices facilitated the creation of a cost-effective and non-invasive microwave heat applicator that could locally heat murine bladder while maintaining normothermic skin and core body temperatures. Since the physical dimensions of the prototype applicator designed in this project can be scaled with frequency to adjust the diameter and depth of heating, the design procedure described in this work may be applied to design similar devices for other small-animal hyperthermia studies.

Materials and Methods

Antenna Design Optimization

The first step in the development of a simulated murine bladder heating model was the creation of an anatomically accurate, 3-dimensional (3D) CAD model of a mouse. Micro-MR images of a female mouse [acquired using a 7T Magnex Scientific magnet] were

obtained from Duke University's Center for In Vivo Microscopy. The images used to create a 3D model have a resolution of 6.25μm resolution in all 3 dimensions. Using Avizo® software package (Visualization Sciences Group, Burlington, MA), the micro-MR images were segmented to yield 3D surfaces for the mouse's body, bladder, vagina, and rectum. These surfaces were assumed to be the outer boundary of a uniform volume of tissue. Once imported into HFSS™ electromagnetic simulation software, frequency-dependent tissue properties, acquired from literature (18), were assigned to each volume. Tissue properties at 2.45GHz are listed in Table I. The mouse was oriented to lie on its back, with the applicator positioned over the pelvis. For the purposes of optimizing the antenna, no significant differences were seen with the addition of typical thickness skin and fat layers between the applicator and bladder.

To achieve adequate power deposition in the bladder with an integrated surface-cooling system, we used a deionized (DI) water-loaded circular waveguide design. The largest diameter tubular waveguide which allows for only a single mode to propagate was selected by sweeping through diameter sizes in 1mm increments. The length of the coaxial monopole feed protruding inside the tube and the distance between the backshort (end plate of waveguide tube) and the coaxial feed were design variables, and a parametric sweep of these variables was performed to optimize the applicator load impedance (S_{11}) when coupled to the pelvis of the mouse and to maximize specific absorption rate (SAR) in the bladder.

Convergence was met when a maximum change of 5% in the S-parameters was achieved between two consecutive adaptive mesh passes. The S_{11} was optimized at less than 1% reflected power for 2.45GHz. Following optimization of the antenna design parameters for load impedance, the local SAR pattern was also determined with HFSS™. Similar to previous work in which an array of patch antennas was optimized to maximize power deposition in a tumor target (19), bladder heating efficiency (η) was defined by integrating the local SAR in the bladder volume and dividing by total SAR in the mouse (Equation 1). This efficiency value was optimized to obtain maximum differential heating of the bladder.

$$\eta = \frac{\int Local \quad SAR * dV_{bladder}}{\int Local \quad SAR * dV_{mouse}} \qquad \text{Equation 1}$$

Because DI water efficiently absorbs electromagnetic power at 2.45GHz, the overall height of the waveguide was minimized to optimize transmission of power into the mouse (S_{21}) and minimize direct heating of the coupling fluid. The water input channel and coaxial connector size required that the height of the waveguide from the center of the coaxial input feed to the circular waveguide output port be at least 15mm. In a circular waveguide, the coaxial feed length and backshort distance determine the resistance and reactance of the waveguide. In a circular waveguide, the optimum backshort distance should be around 0.25λ (3.4mm in our water-loaded waveguide), but the waveguide was constructed with a 1 to 10mm-range adjustable backshort distance so the feed-point reactance could be manually adjusted as needed to impedance match the applicator to the mouse load. This was realized in construction by soldering a copper disk (backshort) to the end of the water output port tube which had a watertight sliding fit in the back end of the circular waveguide. The backshort can then be positioned closer to or further from the coax feed by sliding the water output port in or out of the applicator (see Figure 1).

Thermal modeling

To complete the optimization of a murine bladder heating system, a heat transfer study was implemented in COMSOL Multiphysics®. This study was based on the Pennes Bioheat

Transfer Equation (20) which accounts for all major thermal inputs and outputs of the energy balance in biological tissue, namely, blood perfusion, thermal storage, heat conduction, metabolic heat production and externally applied SAR (calculated in HFSS™).

In the hyperthermia temperature range, both perfusion and metabolism rates increase in response to external applied heating of the targeted tissues. These variations are significant and are accounted for as shown in Equation 2 and Equation 3.

$$\omega_b(T) = (1.9T - 200) * 10^{-6} \quad \text{Equation 2}$$

(21, 22)

$$Q_m(T) = Q_{m0} e^{E_a \frac{(T-T_0)}{k_b T T_0}} \quad \text{Equation 3}$$

(23, 24)

In these expressions temperature (T) is measured in degrees Kelvin, E_a = 0.67eV is the activation energy, k_b is the Boltzmann constant and Q_{m0} = 10760W/m^3 is the basal heat metabolic rate (25).

Anesthesia induces hypothermia which adversely affects the normal thermal regulation of mice, inducing a general drop of 30% in basal metabolism (26). For this reason mice were placed on a heated pad with a constant temperature of 37°C. The rest of the body was exposed to room temperature (25°C) with an assumed convection coefficient of 5W/m^{2}K. The final thermal boundary condition is water bolus temperature, which is expected to play an important role in avoiding the overheating of skin from the externally applied microwave field. All of these considerations were accounted for in this thermal model.

S Parameter and SAR Validation

With a latex membrane sealed over the front opening of the waveguide to contain the circulating water, the applicator was placed adjacent to skin over the pelvis of C57BL/6 mice (Harlan Laboratories, Indianapolis, IN) and S_{11} was measured using an Agilent E5071C network analyzer. The applicator's adjustable backshort-to-coaxial feed distance was varied until an S_{11} of approximately −20dB was obtained for the desired operating frequency of 2.45GHz. To confirm the validity of SAR patterns simulated by HFSS™, the SAR pattern of the applicator was measured with an electric field probe (APREL Laboratories, Ottawa, Ontario, Canada) that was scanned in a tank containing tissue-equivalent liquid with 1mm step size in 3D using procedures that have been published previously (27). The tank contained a mixture of Tween 80 and DI water to create a liquid that simulates muscle tissue at 2.45GHz. The measured dielectric constant was within 5% and the electrical conductivity within 1% of published values (18).

In Vivo Murine Bladder Heating Studies

C57BL/6 mice were anesthetized with an IP injection of 65mg/kg Nembutal and placed on a thin acrylic platform. Underneath the platform, heated water was circulated to help maintain 37°C core body temperature. Heating performance of the applicator was tested in mice with full bladder volumes of approximately 0.15ml at 2-3mm depth. Temperature distributions in the mouse pelvis were characterized by mapping Luxtron® fiber-optic temperature sensors (LumaSense Technologies, Santa Clara, CA) inside three parallel 20Ga polyurethane catheters inserted into the perineum of the mouse and extending 20mm superiorly into the pelvis. The catheters were inserted at depths of 0-1mm, 2-3mm, and 4-5mm below the abdominal wall, with the mid-depth catheter passing immediately adjacent to the bladder.

The sensors were connected to a motor that pulled the sensors out, stopping to allow for a temperature measurement every 1mm and then pushing the sensors back 1.5cm deep again, collecting 15 temperature measurements in each 1 minute cycle. Systemic temperature was measured with a stationary fiber-optic temperature probe inserted orally. The temperatures were collected and displayed in real-time using LabVIEW software (National Instruments, Austin, Texas), which allowed the user to manually control applicator power as needed to maintain the desired temperature distribution in the mouse at all times. All murine *in vivo* studies described in this manuscript were conducted in accordance with the Institutional Animal Care & Use Committee at Duke University.

Results

With the fixed backshort distance of 0.25λ, a parameter sweep in HFSS™ determined the optimal coaxial probe length to be 1.5mm past the center line of the waveguide (6.25mm from sidewall feed-point). Figure 1 shows pictures of the prototype 2450 MHz applicator, the HFSS™ model, and the applicator being used in a murine bladder hyperthermia study.

At 2.45GHz, the dielectric properties of DI water decrease the wavelength from 12.2cm to 13.6mm, with a corresponding decrease in waveguide diameter required for efficient wave propagation. The wave propagation constant was calculated at 1mm increments over a range in diameter from 4-16mm, and a diameter of 9.5mm was selected in order to limit wave propagation to the dominant mode.

After waveguide construction, S_{11} and SAR were measured in homogeneous muscle tissue simulating material and compared to simulated results. The S_{11} simulation results are most accurate (≤ 5%) below 2.6GHz. Figure 2 demonstrates less than 5% difference between simulated and measured S_{11} around the critical 2.45 GHz design frequency, with approximately 1% power reflected at 2.45GHz.

Figure 3 shows that the SAR pattern simulated in HFSS™ matches well to the SAR data that is measured in muscle-equivalent liquid using an E-field scanning probe. The E-field probe contains three orthogonal dipoles centered 3mm from the tip; therefore, SAR patterns are recorded with the closest measurements already 3mm from the antenna front face (Figure 3c). The error between the simulated and measured SAR does not exceed 10%, and applying a moving average window to the simulated data suggests that errors in the side lobe regions may be due to the fact that the diameter of the electric field probe used for SAR measurement is 70% as large as the waveguide aperture.

Simulations of SAR in the mouse model (Figure 4) indicate that maximum power deposition will occur in the skin and subcutaneous tissue directly above the bladder. The temperature of skin and subcutaneous tissue may be lowered by circulating appropriate temperature water coolant through the applicator. This makes fortuitous use of the high dielectric constant water-loading of the waveguide which is also used to reduce waveguide diameter for operation at 2.45GHz.

Figure 5 presents the effect of the water bolus at different temperatures on the resulting temperature profile. It is readily seen that as the surface temperature is decreased the hot spot moves away from the skin surface to the bladder region and the percentage of bladder heated from 42-44°C is increased.

To study the relative heating of all mouse tissues, the corresponding tissue-average temperatures are presented in Figure 6. To restrict the analysis to just the heated region, average rectal and vaginal temperatures were calculated from tissue located within a cylinder of the diameter of the antenna and extending down under the antenna. Figure 6

demonstrates that the rectum is always 1-2°C below the temperature of the vagina and the vagina is always 1-2°C below the temperature of the bladder for bolus temperatures between 35-41°C. These results also indicate that a bolus temperature of 36-38°C will yield the desired temperature range of 42.5-43.5°C in the bladder. For thermosensitive liposomes loaded with mitomycin-C, the assumed target temperature is between 41-43°C, though studies will be conducted with higher and lower bladder temperatures as shown possible in Figure 6.

In vivo murine bladder hyperthermia studies were conducted to validate results seen in simulation. As seen in the Mouse 1 experiment (Figure 7), RF power (15W) was turned on at the 5-minute time point and steady state was reached at the 10 minute time point. At steady state, the subcutaneous tissue was maintained around 40°C due to the cooling effects of 37°C water circulating inside the applicator. Tissues around the bladder and rectum were elevated to 42-43°C while the core body temperature was maintained around 38°C throughout the heating period. The RF power was turned off at the 18-minute time point and the tissue temperature returned to normothermic conditions by the 25-minute time point. The same heating protocol was used for the following four mice, with minor variations in cooling bolus temperature, RF power level, and heat start and stop times.

Discussion

A miniature water-loaded waveguide applicator operating at 2.45GHz was optimized, built and tested. The diameter of the applicator scales with frequency and affects the volume and depth of heating. A 2.45GHz applicator was appropriately sized for heating murine bladder, while lower frequency (larger diameter) applicators would be more ideal for heating larger or deeper regions and higher frequency (smaller diameter) applicators could be designed to heat smaller and more superficial targets. However, when heating deep targets in larger animals such as rabbits and rats, applicator miniaturization is less necessary and existing hyperthermia systems may be considered. For example, a readily-available low frequency (433MHz) horn antenna has been shown to effectively heat rat bladder (28).

The 2.45GHz murine bladder-heating applicator heats small regions at depth (2-3mm) while maintaining normothermic surface and core body temperatures. Other designs were considered, such as the open end of a 6mm diameter semi-rigid coaxial cable; however, the water-loaded circular waveguide was chosen for its overall performance. With a waterbolus naturally integrated into the device itself, this design eliminated the need to construct a separate miniature water bolus for surface cooling.

Bones were not used in the numerical model. They were not visible for segmentation in the micro-MR images and because the pelvic bones in mice are far from the heated region, it was not necessary to include them in this case. Micro-CT images should be considered for future small-animal antenna design and planning studies when bones are in proximity to the treatment region. Measured S_{11} of the prototype applicator matches the simulated S_{11} within 5% at 2.45GHz. The small difference may be explained by the convergence criteria used in simulation; convergence was met when a maximum change of 5% in the S-parameters was achieved between two consecutive adaptive mesh passes. Greater than 5% error at other frequencies is due to the fact that a dispersive model used for the different tissues in the HFSS™ model and convergence of S parameters was only required at the frequency of interest (2.45GHz).

Simulated SAR and measured SAR reveal the same pattern of power deposition in muscle-equivalent liquid. The highest difference between simulated and measured SAR is apparent in the side lobe regions, likely due to the diameter of the electric field probe used to measure

SAR. However, both thermal simulations and measurements confirm that the water cooling eliminates temperature rise in tissues superficial to the bladder and thus negates any deleterious effect that side lobes would have.

In pre-clinical and clinical hyperthermia studies, calculating local SAR is not a good predictor for steady state temperature in the body because it does not account for thermal effects, such as convection and perfusion, which play such an important role in the thermoregulation of rodents. Therefore, thermal models where these effects are taken into account are paramount for predicting treatment outcome. Accurate thermal models require knowledge of the real SAR and power level in the system, as well as the thermal characteristics of all involved biological tissues. Recently, the relation between model and real-world SAR and power levels was successfully realized (29). The effect of heat on perfusion is not well-characterized in highly perfused organs and tissues, and therefore more work is still required before thermal models can be used for clinical hyperthermia treatment planning in various organ and tissue sites. For less perfused organs, such as the bladder, thermal modeling is more achievable.

Figures 4 and 5 were the results of a first attempt to characterize the thermal distribution during a murine bladder hyperthermia study with a thermal model. A difference of 1-2°C between the bladder and the rectum was predicted by this thermal model and validated in *in vivo* experiments (Figure 6), demonstrating that a thermal model may be used to accurately predict internal temperatures during murine hyperthermia studies. Therefore, electromagnetic and thermal simulations can be used as a reliable system design and treatment planning methodology.

A similar difference of 1-2°C between the bladder and the vagina was predicted (Figure 5). Temperature measurements could not be taken inside the bladder, but the results of thermal simulations of water cooled microwave antenna heating indicate that a probe in the vagina can be used as a reliable surrogate for the bladder with an accuracy of ±1°C, where the bladder is always at a higher temperature than what is measured in the vagina. Aside from the results of these thermal simulations, the bladder was assumed to be at temperatures close to or higher than the vagina for two reasons: 1) urine is a more efficient absorber of microwave power than the surrounding tissues, and 2) surrounding tissues experience the cooling effects of blood perfusion more than urine inside the bladder which has no perfusion.

As seen in Figure 7, temperature profiles induced by the bladder hyperthermia treatment looked similar in all five mice. Minor differences in the amount of RF power used and temperature of cooling bolus are seen, likely due to how each mouse's body temperature regulation mechanisms respond under anesthesia. After the hyperthermia treatments, visual inspection of the mouse skin directly under the applicator revealed no burns, as expected from the low measured surface temperatures. In these studies, water bolus temperature was measured at the input port and is likely to be slightly lower than actual skin surface temperature. In future studies, a more accurate measure of skin-bolus interface temperature will be obtained by measuring the temperature of the water flowing from the output port and averaging input and output port temperatures.

We kept body core temperature above 30°C with a temperature controlled water pad placed under the mouse throughout the heat treatment. Due to the fact that mice depend on their tails for thermoregulation, it should be noted that the entire tail of the mouse was placed in direct contact with the temperature-controlled pad. However, the core temperature variations in Figure 6 demonstrate that the temperature-controlled water pad was not a reliable way to regulate body temperature. In future studies, a feedback-controlled constant temperature mat

such as the CMA 450 Temperature Controller (CMA Microdialysis AB, Solna, Sweden) will be used to better maintain core body temperature throughout the heat treatments. A constant temperature boundary under the mouse was used in the thermal simulations. A more reliable method for achieving a constant body temperature experimentally by using a feedback-controlled temperature mat would potentially yield a more reliable method for attaining the internal temperatures seen in Figure 7.

Although varying antenna operating frequency has the most effect on power deposition pattern and volume of heating, another method to control the depth distribution of heating is to vary temperature of the cooling bolus (Figure 5). A lower temperature bolus removes more heat from surface tissues, effectively increasing relative heating at depth. Therefore, this microwave antenna can be used either for heating sub-surface tumors while maintaining cool temperatures in overlying tissue, or by increasing bolus temperature can heat tumors effectively from the surface down to 1.5-2cm depth.

The device described and implemented in this study can form the backbone of a preclinical bladder hyperthermia program. Temperatures achieved in the mouse bladder are quite similar to what we have achieved clinically in patients using the BSD2000 deep regional heating system. The similarity in temperatures achieved will permit pre-clinical studies to be performed that recapitulate the temperatures achieved clinically. Thus the development of this novel hyperthermia device will allow us to screen drugs in bladder tumor bearing mice for their efficacy in combination with heat (30, 31). Additionally, we will be able to study the pharmacokinetics and pharmacodynamics of novel chemotherapeutic drugs packaged in thermally sensitive liposomes thereby refining the tools available for clinical study in humans (32-34).

Conclusion

Until now, there has not been a reliable, cost-effective method to non-invasively heat deep seated small animal targets like murine bladder while maintaining normothermic skin and body core temperatures. To create a microwave heating device specifically for this purpose, we used electromagnetic simulations to optimize the design of miniature water-loaded circular waveguide antennas operating at 2.45GHz. We built an optimized prototype and validated its utility for heating murine bladder with laboratory and pre-clinical measurements. The results from these studies confirm that we have built a low-cost microwave applicator that effectively, and non-invasively, heats murine bladder while maintaining normothermic surface and core body temperatures. This device is now available for pre-clinical studies to investigate the effectiveness of combination heat and chemotherapy treatment of bladder cancer.

Acknowledgments

Research was supported by NIH grant CA42745-21-23 and an NSF Graduate Research Fellowship. Software was supported by Ansys, COMSOL and VSG. The authors would also like to acknowledge Donald V. Pearce Jr. of the Duke University Medical Instrument Shop for his work in constructing the prototype applicators.

References

1. Israel L, Chahinian P, Depierre A. Response of 65 measurable epidermoid bronchogenic tumors of known spontaneous doubling time to four different chemotherapeutic regimens--strategic deductions. Med Pediatr Oncol. 1975; 1(2):83–93. [PubMed: 1228415]
2. Wallner KE, Banda M, Li GC. Hyperthermic enhancement of cell killing by mitomycin C in mitomycin C-resistant Chinese hamster ovary cells. Cancer research. Mar 1; 1987 47(5):1308–12. Research Support, U.S. Gov't, P.H.S. [PubMed: 3102043]

3. Vujaskovic, Z.; Craciunescu, O.; Stauffer, P.; Carroll, M.; Lan, L.; Dewhirst, M., et al., editors. Pilot study of external hyperthermia and intravesical mitomycin-C to treat recurrent bladder cancer after failed standard therapy. Journal of Clinical Oncology; ASCO Annual Meeting; 2010;
4. Joiner MC, Steel GG, Stephens TC. Response of two mouse tumours to hyperthermia with CCNU or melphalan. Br J Cancer. Jan; 1982 45(1):17–26. [PubMed: 7059461]
5. Peller M, Schwerdt A, Hossann M, Reinl HM, Wang T, Sourbron S, et al. MR characterization of mild hyperthermia-induced gadodiamide release from thermosensitive liposomes in solid tumors. Invest Radiol. Dec; 2008 43(12):877–92. [PubMed: 19002060]
6. Hill SA, Denekamp J. The effect of vascular occlusion on the thermal sensitization of a mouse tumour. Br J Radiol. Dec; 1978 51(612):997–1002. [PubMed: 737414]
7. Meyer DE, Shin BC, Kong GA, Dewhirst MW, Chilkoti A. Drug targeting using thermally responsive polymers and local hyperthermia. J Control Release. Jul 6; 2001 74(1-3):213–24. [PubMed: 11489497]
8. Mukhopadhaya A, Mendecki J, Dong X, Liu L, Kalnicki S, Garg M, et al. Localized hyperthermia combined with intratumoral dendritic cells induces systemic antitumor immunity. Cancer Res. Aug 15; 2007 67(16):7798–806. [PubMed: 17699785]
9. Marmor JB, Hilerio FJ, Hahn GM. Tumor eradication and cell survival after localized hyperthermia induced by ultrasound. Cancer Res. Jun; 1979 39(6 Pt 1):2166–71. [PubMed: 445414]
10. Marmor JB, Hahn N, Hahn GM. Tumor cure and cell survival after localized radiofrequency heating. Cancer Res. Mar; 1977 37(3):879–83. [PubMed: 837383]
11. Nomura S, Mukasa S, Yamasaki H, Maehara T, Aono H, Kikkawa H, et al. Inductive heating of mg ferrite powder in high-water content phantoms using AC magnetic field for local hyperthermia. Heat Transfer Eng. 2007; 28(12):1017–22.
12. Maehara T, Konishi K, Kamimori T, Aono H, Naohara T, Kikkawa H, et al. Heating of ferrite powder by an AC magnetic field for local hyperthermia. Jpn J Appl Phys 1. Mar; 2002 41(3A): 1620–1.
13. Attaluri A, Ma RH, Qiu Y, Li W, Zhu L. Nanoparticle distribution and temperature elevations in prostatic tumours in mice during magnetic nanoparticle hyperthermia. International Journal of Hyperthermia. 2011; 27(5):491–502. [PubMed: 21756046]
14. Sonvico F, Mornet S, Vasseur S, Dubernet C, Jaillard D, Degrouard J, et al. Folate-conjugated iron oxide nanoparticles for solid tumor targeting as potential specific magnetic hyperthermia mediators: Synthesis, physicochemical characterization, and in vitro experiments. Bioconjugate Chem. Sep-Oct;2005 16(5):1181–8.
15. James BJ, Sullivan DM. Creation of three-dimensional patient models for hyperthermia treatment planning. IEEE Trans Biomed Eng. Mar; 1992 39(3):238–42. Research Support, U.S. Gov't, P.H.S. [PubMed: 1555853]
16. James BJ, Sullivan DM. Direct Use of Ct Scans for Hyperthermia Treatment Planning. Ieee T BioMed Eng. Aug; 1992 39(8):845–51.
17. Gellermann J, Wust P, Stalling D, Seebass M, Nadobny J, Beck R, et al. Clinical evaluation and verification of the hyperthermia treatment planning system HyperPlan. Int J Radiat Oncol. Jul 1; 2000 47(4):1145–56.
18. Gabriel, C. Compilation of the dielectric properties of body tissues at RF and microwave frequencies. In: Brooks Air Force Base. , editor. Occupational and environmental health directorate RRD. Texas (USA): 1996.
19. Trefna HD, Vrba J, Persson M. Evaluation of a patch antenna applicator for time reversal hyperthemia. International Journal of Hyperthermia. 2010; 26(2):185–97. [PubMed: 20146572]
20. Pennes HH. Analysis of Tissue and Arterial Blood Temperatures in the Resting Human Forearm. J Appl Physiol. 1948; 1(2):93–122. [PubMed: 18887578]
21. Song, C.; Choi, I.; Nah, B.; Sahu, S.; Osborn, J. Microvasculature and perfusion in normal tissues and tumors. In: Seegenschmiedt MH, FP.; Vernon, CC., editors. Thermoradiotherapy and thermochemotherapy. Springer-Verlag; Berlin, New York: 1995. p. 139-59.
22. Diller, K.; Valvano, J.; Pearce, J. The CRC Handbook of Mechanical Engineering. Second Edition. DYG, FK., editor. CRC Press; 2005.

23. Gillooly JF, Brown JH, West GB, Savage VM, Charnov EL. Effects of size and temperature on metabolic rate. Science. Sep 21; 2001 293(5538):2248–51. [PubMed: 11567137]
24. Gordon C. Quantifying the instability of core temperature in rodents. Journal of Thermal Biology. 2009; 34(5):213–9.
25. Barclay C, Woledge R, Curtin N. Effects of UCP3 genotype, temperature and muscle type on energy turnover of resting mouse skeletal muscle. Pflug Arch Eur J Phy. Feb; 2009 457(4):857–64.
26. Sessler DI. Temperature monitoring and perioperative thermoregulation. Anesthesiology. Aug; 2008 109(2):318–38. [PubMed: 18648241]
27. Neuman DG, Stauffer PR, Jacobsen S, Rossetto F. SAR pattern perturbations from resonance effects in water bolus layers used with superficial microwave hyperthermia applicators. International Journal of Hyperthermia. 2002; 18(3):180–93. [PubMed: 12028636]
28. Haveman J, Smals OAG, Rodermond HM. Effects of hyperthermia on the rat bladder: a pre-clinical study on thermometry and functional damage after treatment. International Journal of Hyperthermia. 2003; 19(1):45–57. [PubMed: 12519711]
29. de Bruijne M, Samaras T, Chavannes N, van Rhoon GC. Quantitative validation of the 3D SAR profile of hyperthermia applicators using the gamma method. Phys Med Biol. Jun 7; 2007 52(11): 3075–88. [PubMed: 17505090]
30. Gunther JH, Jurczok A, Wulf T, Brandau S, Deinert I, Jocham D, et al. Optimizing syngeneic orthotopic murine bladder cancer (MB49). Cancer Res. Jun 15; 1999 59(12):2834–7. [PubMed: 10383142]
31. Yamada H, Matsumoto S, Matsumoto T, Yamada T, Yamashita U. Murine IL-2 secreting recombinant Bacillus Calmette-Guerin augments macrophage-mediated cytotoxicity against murine bladder cancer MBT-2. J Urol. Aug; 2000 164(2):526–31. [PubMed: 10893638]
32. Chen Q, Krol A, Wright A, Needham D, Dewhirst MW, Yuan F. Tumor microvascular permeability is a key determinant for antivascular effects of doxorubicin encapsulated in a temperature sensitive liposome. Int J Hyperthermia. Sep; 2008 24(6):475–82. [PubMed: 18608573]
33. Lindner LH, Eichhorn ME, Eibl H, Teichert N, Schmitt-Sody M, Issels RD, et al. Novel temperature-sensitive liposomes with prolonged circulation time. Clin Cancer Res. Mar 15; 2004 10(6):2168–78. [PubMed: 15041738]
34. Tacker JR, Anderson RU. Delivery of antitumor drug to bladder cancer by use of phase transition liposomes and hyperthermia. J Urol. Jun; 1982 127(6):1211–4. [PubMed: 7087041]

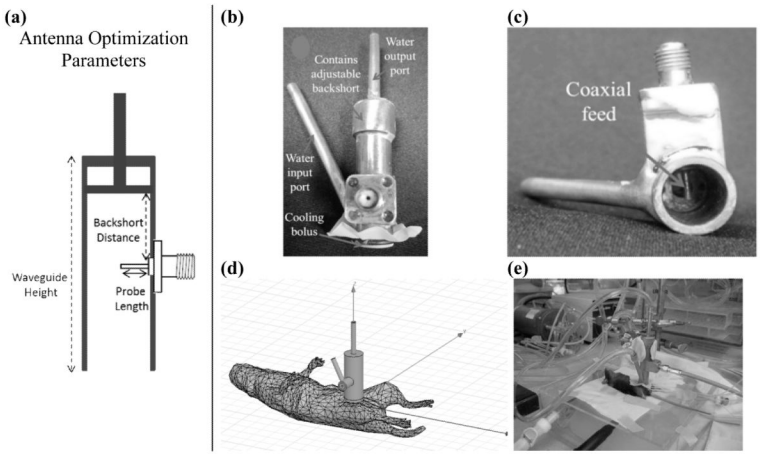

Figure 1.

a) Parameters varied to optimize SAR and S_{11}; b) Front-view picture of 2.45GHz applicator; c) Bottom-view picture of 2.45GHz applicator; d) HFSS™ model of applicator on mouse; e) Snapshot of experimental setup for murine bladder hyperthermia study with applicator positioned on the skin overlying the pelvis.

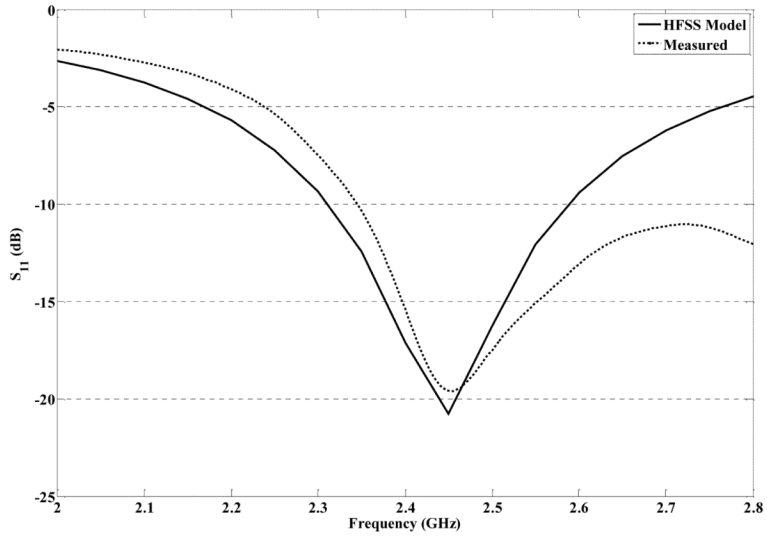

Figure 2.
S_{11}: HFSS™ simulation compared to measurements using an Agilent E5071C network analyzer.

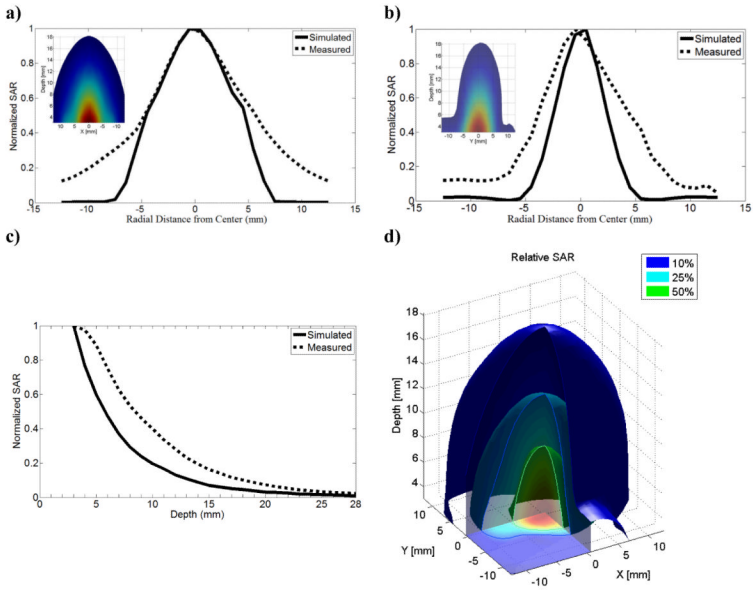

Figure 3.

SAR: HFSS™ simulation compared to measurements with all values normalized to the maximum value at 3mm depth: a) profile across x-axis, b) profile across y-axis, c) depth profile, and d) 3D SAR measurements in muscle phantom

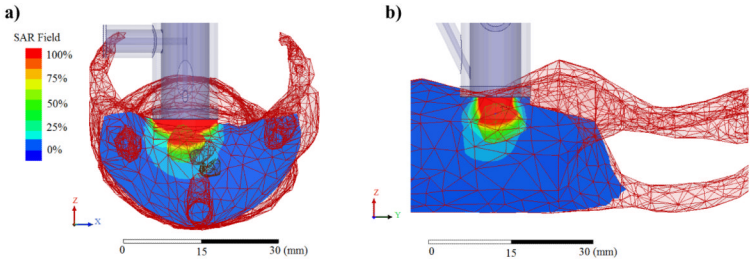

Figure 4.
HFSS™ SAR simulation in mouse model a) x-axis profile and b) y-axis profile

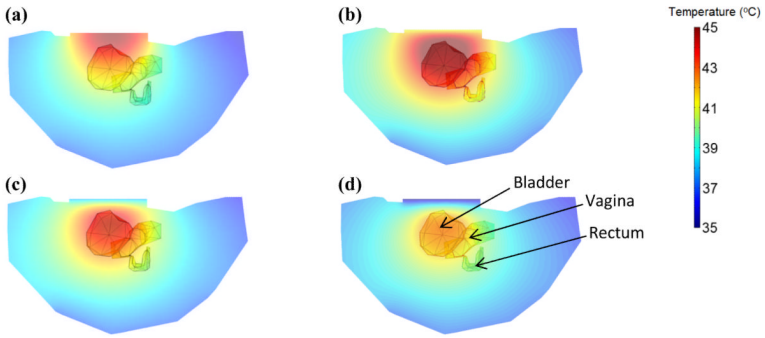

Figure 5.
2D slice temperature profiles in mouse body, bladder, vagina and rectum with bolus temperature (a) unregulated (b) constant 41°C, (c) constant 38°C and (d) constant 35°C and RF power set at (a) 5W and (b), (c), (d) 12W.

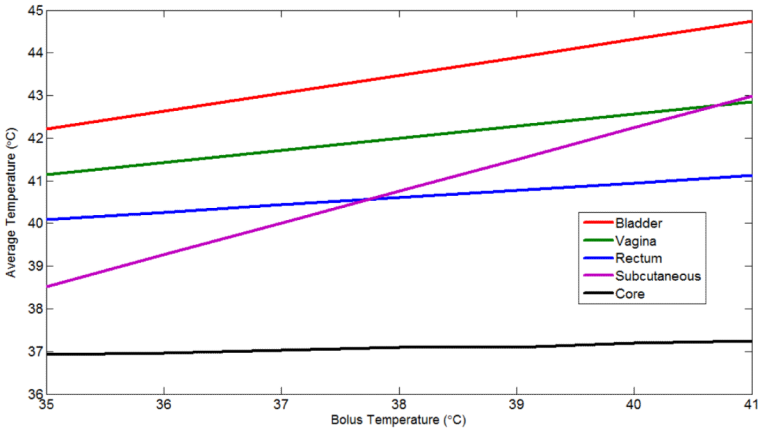

Figure 6.
COMSOL simulation of average temperatures as a function of bolus temperature

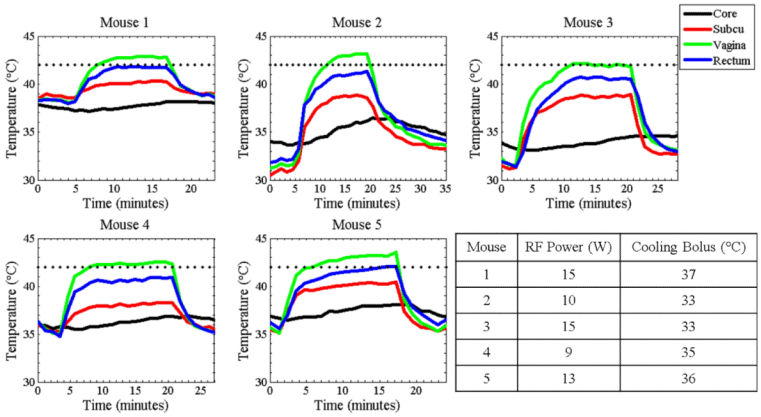

Mouse	RF Power (W)	Cooling Bolus (°C)
1	15	37
2	10	33
3	15	33
4	9	35
5	13	36

Figure 7.

Temperature data taken from five independent murine bladder hyperthermia studies. Temperature increases occur when RF power is turned on (around the 2-5minute mark) and decreases occur when RF power is turned off (around the 18-20minute mark). The dotted line signifies 42°C.

Table I

Properties of murine tissues at 2.45GHz[18]

	Dielectric onstant , ε	**Electrical Conductivity, σ (S/m)**	**Specific Heat, C_p (J/kg°C)**	**Thermal Conductivity, k (W/m°C)**	**Density, ρ (kg/m^3)**
Body (muscle)	52.729	1.7388	3546	0.53	1041
Bladder (urine)	71.238	7.4257	4200†	0.561	1000
Uterus	57.814	2.2465	3580	0.50	1052
Colon	53.879	2.0383	3653	0.56	1044

†Urine and water have similar thermal conductivity and density values, so we assume that the specific heat of urine is also similar to water.